Journal of Power Sources 196 (2011) 9322–9330

Contents lists available at ScienceDirect

Journal of Power Sources

journal homepage: www.elsevier.com/locate/jpowsour

Insight into the grain boundary effect on the ionic transport of yttria-stabilized zirconia at elevated temperatures from a molecular modeling perspective

Kai-Shiun Chang, Yi-Feng Lin, Kuo-Lun Tung*

R&D Center for Membrane Technology and Department of Chemical Engineering, Chung Yuan Christian University, 200 Chung-Pei Road, Chungli, Taoyuan 32023, Taiwan

ARTICLE INFO

Article history:
Received 22 June 2011
Received in revised form 29 July 2011
Accepted 30 July 2011
Available online 5 August 2011

Keywords:
Molecular dynamics
Yttria-stabilized zirconia
Grain boundary
Solid electrolyte
SOFC

ABSTRACT

A molecular dynamics (MD) simulation is used to reveal the grain boundary effect on the ionic transport of yttria-stabilized zirconia (YSZ). The oxygen ion displacements and diffusivities of the ideal and grain boundary-inserted YSZ models are analyzed at elevated temperatures. An optimized Y_2O_3 concentration within YSZ for the best ionic conductivity is achieved by balancing the trade-off between the increased vacancies and the decreased accessible free space. The mass transfer resistance of the grain boundary in YSZ can be more easily found at higher temperatures by observing the oxygen ion diffusivities or traveling trajectories. At lower temperatures, the grain interior and the grain boundary control the ionic transport. In contrast, the grain boundary effect on the diffusion barrier is gradually eliminated at elevated temperatures. The modeled results in this work agree well with previous experimental data.

1. Introduction

Yttria-stabilized zirconia (YSZ) solid electrolytes and materials derived from them have widely been used for solid oxide fuel cell applications because of their excellent durability for long-term use. In order to improve the balance between performance and durability, previous studies have attempted to design this material from the perspective of the material composition of zirconia [1–14]. The grain boundary (GB) in the resultant solid electrolyte exhibits an apparently higher resistance than the grain interior (GI) [15], which could be attributed to the aggregation of complex defects near the grain–grain interface regions [16]. Therefore, the presence of GBs lowers the overall ionic conductivity because they are intrinsically unfavorable to ion transport. As a result, previous studies have analyzed ionic transport in the GIs and GBs of zirconia-based solid electrolytes [17–19]; however, some studies have suggested that the interfacial area between two grains may form a channel for ionic transport with the proper structural design [20,21], which also indicates the importance of the properties of GBs for ionic transport. As a result, GBs also play a vital role in the ionic conduction of the solid electrolyte at an intermediate temperature for SOFC applications; however, the transport mechanisms of oxygen ions across the GI and GBs are not easy to investigate at an atomic scale using experimental methods. Molecular simulation techniques have proven to be a promising tool in the characterization of organic, inorganic, and hybrid materials at a microscopic level [22–30]. The molecular dynamics (MD) technique can be used to successfully describe how doped species alter the ionic conductivities of zirconia-based solid electrolytes. The discussed factors include the size of the cations, the barrier edge, the defect complex, interionic interactions, and the associated external forces [29–34]. Additionally, phase composition and structural stability were analyzed using MD simulations, and the results were observed to agree well with experimental results [35,36]. Some MD studies have constructed molecular models in order to analyze the ion displacement phenomenon of the GBs in YSZ at temperatures greater than 1273 K, which suggests that GBs typically block oxygen ion transport [37,38]; however, the effect of GBs on ion transport in the intermediate temperature region on a microscopic scale is not fully understood. Thus, this work constructed a molecular model in order to study the effect of GBs on ionic transport mechanisms in YSZ. We developed a molecular model of a YSZ structure with several GBs, such that the ionic diffusion mechanism therein was analyzed and compared with an ideal YSZ model (without GBs). In this work, all the simulations were processed using the Materials Studio package from Accelrys. The details of the model construction and the physical property analyses are described in the following section.

2. Theoretical method

2.1. Model construction

The zirconia-based molecular model was constructed using the cubic zirconia unit, as shown in Fig. 1(a). In this work, a molecular

* Corresponding author. Tel.: +886 3 265 4129; fax: +886 3 265 4199.
E-mail address: kuolun@cycu.edt.tw (K.-L. Tung).

0378-7753/$ – see front matter © 2011 Elsevier B.V. All rights reserved.
doi:10.1016/j.jpowsour.2011.07.085

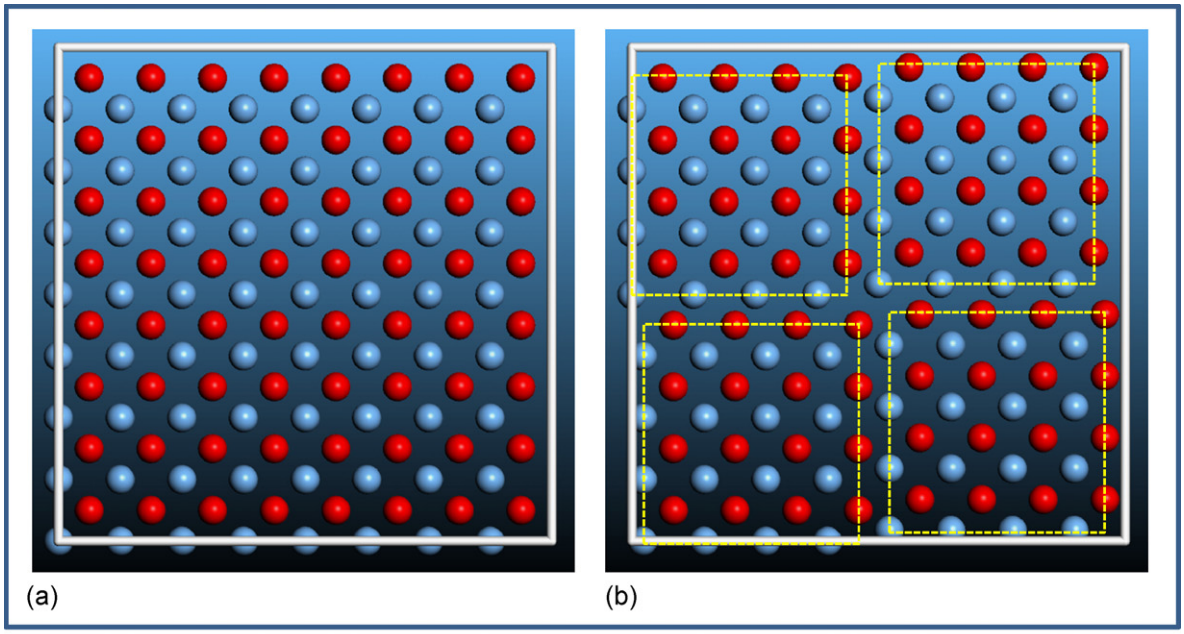

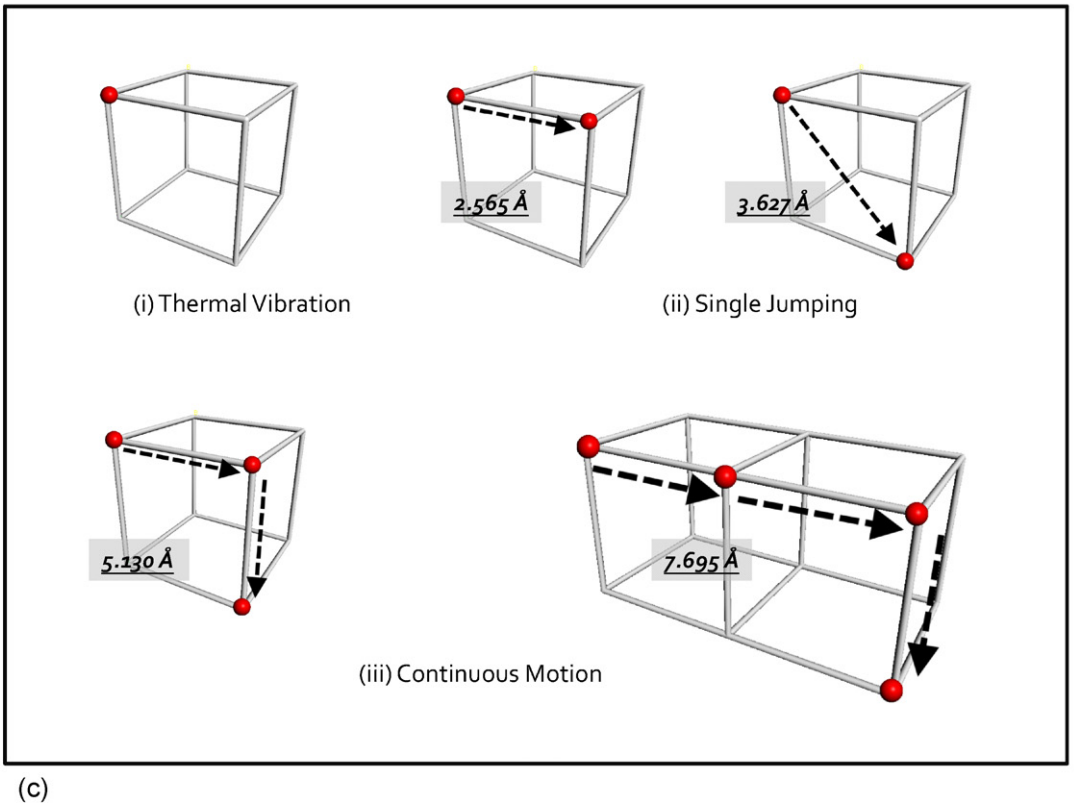

Fig. 1. Schematic expression of the (a) grain-free, (b) grain boundary-inserted molecular models, and (c) oxygen ion moving trajectory types in the sub-lattice of cubic zirconia structure.

model consisting of 64 unit cells was built to be the basis of the YSZ model. Subsequently, different amounts of Y_2O_3 were added to our basis model to replace the original ZrO_2 units so as to form the YSZ structures with different Y_2O_3 concentrations. Specific quantities of vacancies were produced using the following process:

$$YO_{1.5} \xrightarrow{ZrO_2} Y''_{Zr} + \frac{3}{2}O_O + \frac{1}{2}V''_O, \quad (1)$$

The positions of the Zr ions that were replaced by the Y ions were randomly assigned in the YSZ structures with different doping concentrations. Vacancies were formed by randomly removing specific amounts of oxygen ions in the system. Five independent molecular models were constructed and were adopted in order to calculate the average physical properties.

Six types of YSZ models with different Y_2O_3 concentrations were constructed in order to optimize the doping concentration. Table 1 summarizes the model parameters in detail.

Table 1
Parameters of the YSZ molecular models.

Model	Y_2O_3 (mol%[a])	Zr^{+4}/ZrO_2 (no.)	Y^{+3}/Y_2O_3 (no.)	O^{-2} (no.)	V^a (no.)
06-YSZ	6.22	226/226	30/15	497	15
07-YSZ	7.11	222/222	34/17	495	17
08-YSZ	8.02	218/218	38/19	493	19
09-YSZ	8.94	214/214	42/21	491	21
10-YSZ	10.34	208/208	48/24	488	24

[a] Mol% of Y_2O_3 = 100 × (mole no. of Y_2O_3)/(mole no. of Y_2O_3 + mole no. of ZrO_2).

Later, in order to simulate the effect of grain boundaries on ionic transport in the YSZ model, we manually shifted part of the YSZ model structure in the direction of the *x*-axis so as to create slipped dislocations in the molecular model. The slipping distance was set to 0.4436 Å, which effectively reflected the grain boundary effect on the YSZ model in this work. Four subregions were divided by rearranging the ion positions in the space, as shown in Fig. 1(b). It was assumed that these space rearrangements in a cubic structure model expressed the characteristics of a polycrystalline YSZ structure. In addition, in order to maintain the 'inserted-grain boundary structure' for the duration of the MD simulation, several cations were fixed in the YSZ model during the calculation. All the YSZ models were processed using a 500-ps MD duration from 873 K to 1473 K under an NVT ensemble (a fixed atom number, cell volume, and system temperature).

2.2. Potential function

The Born–Mayer–Buckingham potential was adopted in order to illustrate the metal oxide structure and ionic transport behaviors of the binary or mixed oxide doped zirconia system, as follows:

$$j(r_{ij}) = A_{ij}\exp\left(-\frac{r_{ij}}{\rho_{ij}}\right) - \frac{C_{ij}}{r_{ij}^6} + u_{\text{Coulomb}}, \quad (2)$$

where A_{ij}, C_{ij}, and ρ_{ij} are the coefficients that are used in the potential equation. In Eq. (2), the interaction potential between two atoms, *i* and *j*, including the van der Waals (first two terms) and Coulombic (third term) energies, are described. In addition, in Eq. (2), r_{ij} represents the distance between ions *i* and *j*, and u_{Coulomb} represents the Coulombic term. The associated parameters for the theoretical calculations in this work were validated using empirical fittings from previous studies that have investigated zirconia-based structures [39,40], as shown in Table 2.

2.3. Physical property analysis

In our simulation, five independent molecular models were constructed in order to analyze physical properties and obtain average calculated values. The reproducibility was also confirmed in order to validate that this was a reasonable simulation procedure.

Table 2
The potential parameters that were used in the Born–Mayer–Buckingham potential in this study.

Ion pair	A_{ij} (kcal mol^{-1})	ρ_{ij} (Å)	C_{ij} (kcal Å^6 mol^{-1})	Reference
Zr–Zr	0	1	0	
Zr–Y	0	1	0	
Y–Y	0	1	0	
Zr–O	22717.937	0.376	0	[40]
Y–O	30995.940	0.349	0	[39]
O–O	524480.535	0.149	642.704	[40]

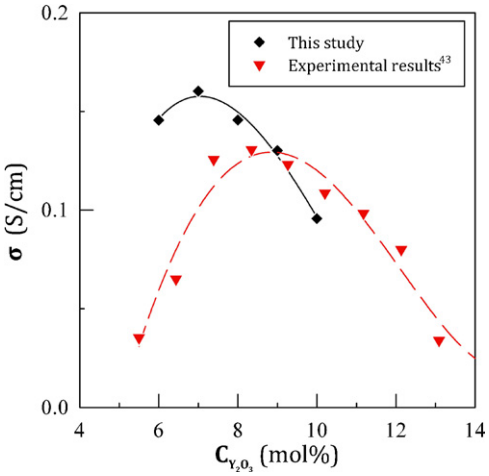

Fig. 2. Ionic conductivity values from this simulation and experimental work [35] at 1273 K.

2.3.1. Mean-squared displacement (MSD) and self-diffusivity

The diffusion mechanism and self-diffusivity of oxygen ions in the YSZ system were analyzed using mean-squared displacement (MSD), which can be defined using the Einstein relationship:

$$\text{MSD}\ (t) = \frac{1}{N}\sum_{i=1}^{N}\left\langle [r_i(t_0+t) - r_i(t_0)]^2\right\rangle = B + 6D\times t \quad (3)$$

where *N* is the total number of atoms; $r_i(t_0+t)$ and $r_i(t_0)$ are the positions at time t_0+t and time t_0, respectively; *B* is a constant; and *D* is the self-diffusivity. The self-diffusivity can be obtained as the slope of the MSD curve versus the elapsed time. The diffusivity ratios of oxygen ions between the M-07-YSZ and P-07-YSZ models can be estimated using the follow equation:

$$\text{Diffusivity ratio} = \frac{\text{Oxygen ion diffusivity of P-07-YSZ}}{\text{Oxygen ion diffusivityof M-07-YSZ}}, \quad (4)$$

2.3.2. Ionic conductivity

The ionic conductivity can be estimated from the diffusion coefficient of oxygen ions using the Nernst–Einstein relationship expressed by the following equation:

$$\sigma = \frac{Nq^2D}{k_B T H_R}, \quad (5)$$

where σ is the ionic conductivity, *N* is the number of oxygen ions in the calculation model, *q* is the electrical charge of the ions, *D* is the diffusion coefficient, k_B is the Boltzmann constant, *T* is the operation temperature, and H_R is the Haven coefficient, which was set at 0.65 in this study [41].

2.3.3. Ion movement distribution

During the MD simulation, the actual ionic moving distance of each oxygen ion can be estimated using its initial and final coordinates. The statistics of each moving distance and the corresponding quantity were collected to express the distribution of ion movement. The moving distances of ions can be compared with the oxygen–oxygen distances in the cubic zirconia unit, which can then be categorized as one of several different movement types, as shown in Fig. 1(c).

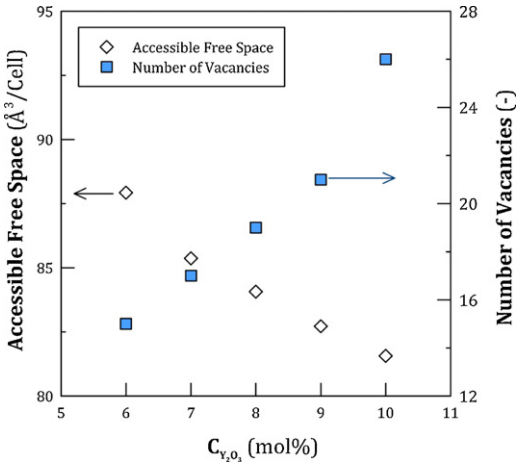

Fig. 3. Accessible free space and vacancy numbers of YSZ models with various Y_2O_3 concentrations at 1273 K.

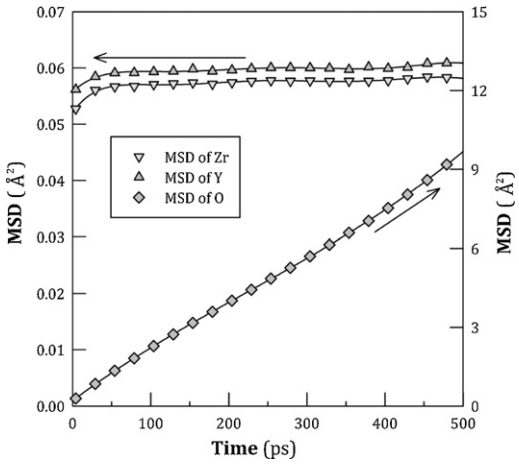

Fig. 4. MSD diagrams of zirconium, yttrium, and oxygen ions in 07-YSZ at 1273 K.

3. Results and discussion

3.1. Oxygen ion transport in ideal YSZ model

Fig. 2 shows the oxygen ionic conductivities of ideal YSZ models with different doped Y_2O_3 concentrations. In Fig. 2, it can be clearly seen that the 07-YSZ revealed the highest ionic conductivity among all the YSZ models with different compositions. In the YSZ structure, increasing the doped Y_2O_3 would release more vacancies. The increased vacancies from adding Y_2O_3 to the YSZ structure tended to form the pathways for oxygen ion transport, which is beneficial for improving the ionic conductivity. However, while the Y_2O_3 concentration is higher than 7 mol%, there is a paradox between the elevated vacancy number and the ionic conductivity, as shown in Fig. 2. The optimized Y_2O_3 concentration of YSZ for ionic transport was approximately 7 mol% in this work. From the past studies, it was determined that the excess Y^{+3} in the YSZ system tended to trap the vacancies, which lowered the vacancy mobility. Thus, oxygen ion mobility was also inhibited, which led to a less effective thermal motion [30,31]. In addition, some studies also pointed out that the Y–Y edge formed in the YSZ system also hampered the oxygen ion movement and then decreased the ion mobility [29–31,42]. As a result, an optimized Y_2O_3 concentration for the YSZ structure would be found. Meanwhile, we also found that the 07-YSZ model provided the best ionic conductivity, which was similar to previous experimental results [43], as shown in Fig. 2. Thus, the 07-YSZ model was adapted for the analysis of the impact of grain boundaries on ionic transport behavior in this study. However, we can still found some differences between the simulated and experimental ionic conductivities of YSZ at various Y_2O_3 concentrations. The reasons of causing this error in our simulation work might be explained by the following descriptions. Firstly, the dimension of the simulated model and the MD duration adopted in this work are less than that of the real system due to the limited computational resources presently. Meanwhile, some intrinsic errors in the calculation process might still be produced by the selected potential function and parameters optimized from the semi-empirical equations. Here, the comparable quantitative results between the simulation and experimental works can be observed, which suggests that the MD simulation can be a useful for the prediction of ionic transport ability of zirconia-based solid electrolytes.

Meanwhile, we also discussed the optimized Y_2O_3 concentration in YSZ for the best ionic conductivity from the perspective of free volume. Fig. 3 illustrates the number of vacancies and the accessible free space (AFS) corresponding to the Y_2O_3 concentrations of YSZ models. The AFS value can be obtained by probing the available space for a hard, spherical particle passing through a YSZ model, where the radius of the probe was set as that of the oxygen ion. A higher AFS value indicates more and larger internal spaces or a higher connectivity among the vacancies in the YSZ structure, which might improve ionic transport. However, it should also be noted that the AFS decreased with the increase of Y_2O_3 in the YSZ models. This reduction of AFS with the increase of vacancies suggested that the connectivity of vacancies might be reduced, or the pathway of oxygen ions might be hindered by raising the Y_2O_3 concentration. Moreover, the distribution of vacancies in higher YSZ concentration systems might not be suitable for the formation of continuous ion motion, which is not favorable when trying to produce better ionic transport. In contrast, the increased Y_2O_3 content would also enlarge the lattice constant of the YSZ structure because of the larger radius of the yttrium ion, which led to the expansion of the molecular model. The expansion of the YSZ structure might also increase the free space in the system. Thus, we checked the lattice parameters of 6 mol% and 10 mol% YSZ from the past theoretical and experimental works [31]. The ratio of lattice parameter of 10 and 6 mol% YSZ is approximately 1.0019. This extent of free space expansion would not alter the results of the AFS analysis in this work, as shown in Fig. 3.

In addition, the displacements of zirconium and yttrium ions in the 07-YSZ model were much smaller than those of oxygen ions, as illustrated in Fig. 4. During the 500-ps MD simulation, the overall displacements of zirconium and yttrium ions were both approximately 0.06 Å, whereas those of oxygen ions were much higher at 10 Å. The cations may have been nearly fixed or may have fluctuated around the lattice sites. Thus, it was assumed that partially fixed cations did not affect the transport of oxygen ions in the YSZ model. In this work, the grain boundary model is referred to as 'P-07-YSZ', whereas the ideal YSZ model is referred to as 'M-07-YSZ'.

3.2. GB effect on oxygen ion MSD and movement

To compare the ion mobility in YSZ structures between the ideal and GB-inserted models, their MSD diagrams were analyzed, as illustrated in Fig. 5. In Fig. 5, it can be clearly seen that the P-07-YSZ model showed lower MSD slopes and displacements during the 500-ps calculation. Because the P-07-YSZ model was also composed of pure cubic-phase units, the structure of the P-07-YSZ model was no different from that of M-07-YSZ, except for the presence of a "grain boundary." Therefore, this lower ion mobility of P-07-YSZ might be caused by the migration barrier from the inserted GBs. The slipped dislocations inside P-07-YSZ formed the ion transport

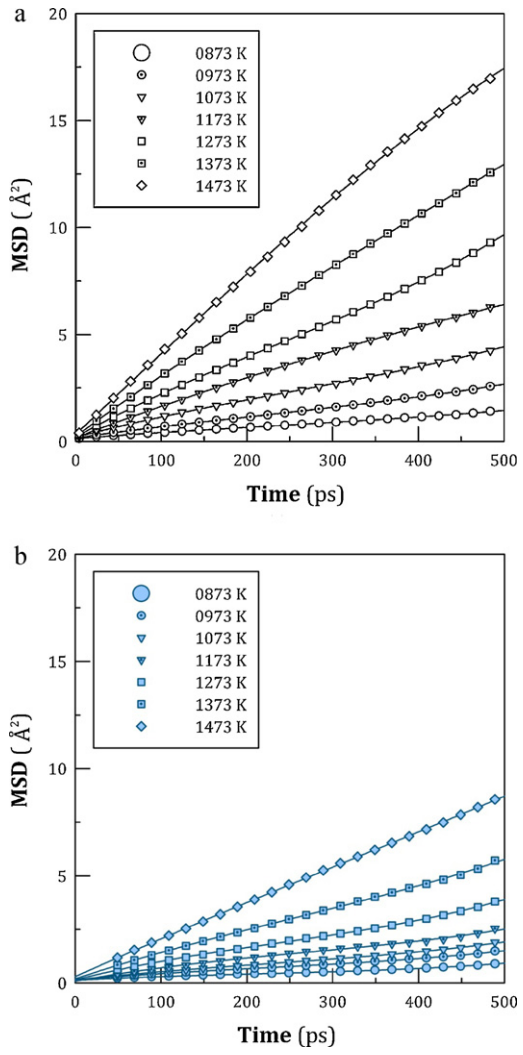

Fig. 5. MSD diagrams of the (a) M-07-YSZ and (b) P-07-YSZ models at different temperatures.

resistance, which hindered partial ionic hopping from one site to another. Thus, the concept of inserted grain boundary can be validated here via the MSD diagram analysis. In order to compare the transport behaviors of oxygen ions in the P-07-YSZ model with those in the M-07-YSZ model, we estimated the absolute values of displacements of all oxygen ions in both models. Fig. 6 illustrates the oxygen ion displacement values of the M-07-YSZ and P-07-YSZ models. These displacement values can be roughly classified into three categories: below 1 Å, between 2 and 6 Å, and beyond 6 Å. In the region between 2 and 6 Å, it can be observed that M-07-YSZ had a higher value than that of P-07-YSZ. M-07-YSZ contained more displacements with high values in comparison with those of P-07-YSZ, which indicates its higher transport ability for oxygen ions. Moreover, a number of oxygen ions with long-distance movement (larger than 8 Å) can be observed in M-07-YSZ (Fig. 6(a)), whereas no such oxygen ions can be observed in P-07-YSZ (Fig. 6(b)). Thus, it can be inferred that the GBs resisted ionic transport and inhibited continuous ionic movements.

Fig. 7 depicts the displacement distribution of oxygen ions in the M-07-YSZ and P-07-YSZ models. In Fig. 7, the P-07-YSZ model exhibits a higher percentage of displacement values that are located in the region of 0–1 Å in comparison with the M-07-YSZ model. More specifically, a higher number of ion vibrations or ion fluctuations were observed in the YSZ model with GBs. This higher ion immobility can be attributed to the barrier that is formed by the

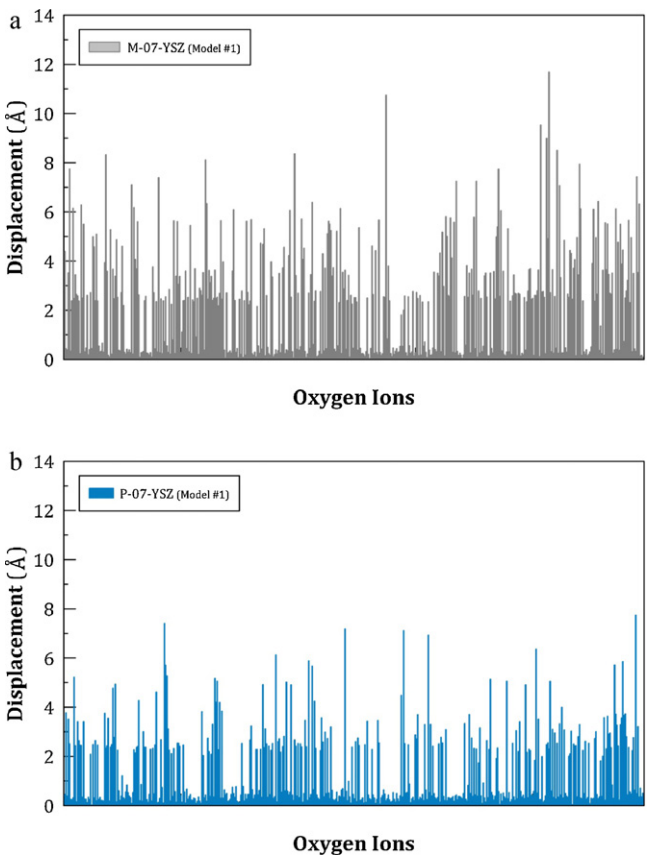

Fig. 6. Oxygen ion displacements during 500-ps MD simulations using the (a) M-07-YSZ and (b) P-07-YSZ models at 1273 K.

GBs. Even though vacancies or mobile oxygen ions were formed near the GBs during the model creation process, the higher mass resistances of the GBs impeded their ability to travel across the boundary. Therefore, the percentage of immobile oxygen ions was higher because of the GBs. In contrast, the M-07-YSZ model exhib-

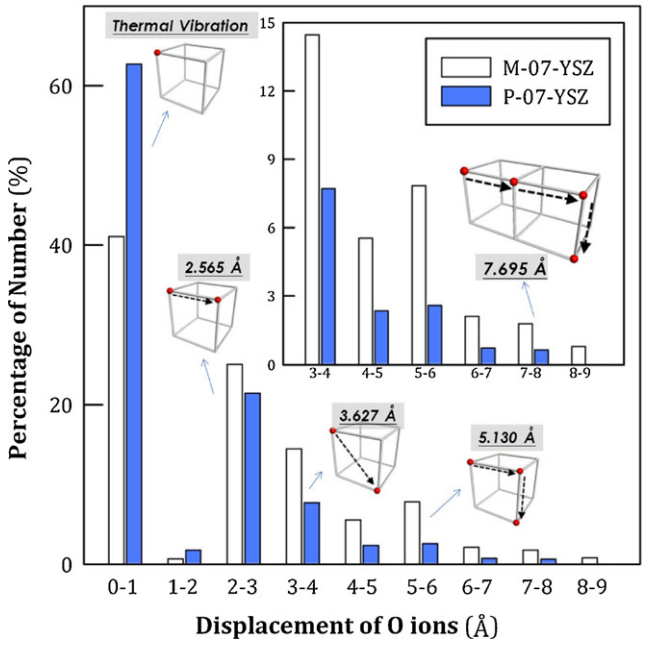

Fig. 7. Comparison of the oxygen ion displacement profiles of the M-07-YSZ and P-07-YSZ models during 500-ps MD simulations at 1273 K.

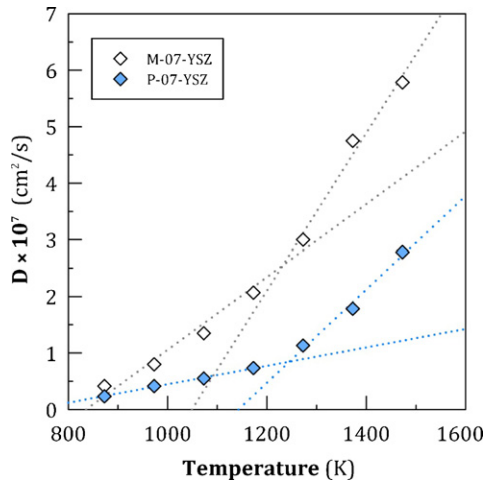

Fig. 8. Oxygen ion diffusivities of the (a) M-07-YSZ and (b) P-07-YSZ models at different temperatures.

ited more high-displacement ions (a displacement value of greater than 3 Å) than the P-07-YSZ model, which indicates better ionic transport in the ideal model. In comparison with the ideal cubic YSZ model, the model with the GBs suggested a method of oxygen ion transport exists in the YSZ structure, with results that were similar to previously obtained experimental results.

3.3. GB effect on oxygen ion diffusivity

The diffusivities of oxygen ions in the M-07-YSZ and P-07-YSZ models were also estimated in this study, as illustrated in Fig. 8. In Fig. 8, the oxygen ion diffusivities of the two models were improved with increases in temperature. Moreover, higher temperatures were observed to increase the kinetic energy, which also increases ion velocity and directs ion movement. Furthermore, the differences in the oxygen ion diffusivities between the M-07-YSZ and P-07-YSZ models were observed to increase with increased temperature, which indicates that the effect of the GBs on oxygen ion transport can be more easily observed at elevated temperatures. The enhanced differences in the oxygen ion diffusivities that accompanied elevated temperatures may be explained by the following phenomenon. In the case of a fluorite-structured solid electrolyte, ionic conduction is induced when the material is heated to 1073 K (CeO_2-based) or 1273 K (ZrO_2-based). In other words, at lower temperatures, ion migrations might not be clearly observable. In this situation, both the M-07-YSZ and P-07-YSZ models exhibited lower ion diffusivities. The effect of the GBs on diffusivity is therefore not apparent in the P-07-YSZ model. At higher temperatures, the oxygen ions in the P-07-YSZ model demonstrated enhanced long-distance transport. The probability of ion interaction with the GBs also increased. Therefore, intergrain resistance was dominant in this scenario.

In contrast, in the M-07-YSZ model, oxygen ion transport was primarily impacted by GI resistance, and a higher energy (due to a higher temperature) would permit the ions to overcome the intragrain barrier, regardless of temperature. Therefore, the differences between the ideal and the GBs-inserted model were substantial with increases in temperature. In addition, we observed a break point at approximately 1273 K by using a regression of the diffusivity values (M-07-YSZ) in Fig. 8, which approached the temperature that is required to induce a high diffusivity. A similar result was observed in the P-07-YSZ model. The obvious increases in diffusivity indicate that the impact of GBs on ion migration might be easier to observe at higher temperatures.

Unfortunately, it is difficult to discuss the extent of the influence of the GBs on ion migration by directly observing differences in diffusivity. A direct comparison of diffusivity differences may not consider how the ionic transport capability of the P-07-YSZ model differs from that of the M-07-YSZ model based on the performance of the M-07-YSZ model. Therefore, in order to explain the associated ion transport mechanism, we calculated the ratios of the

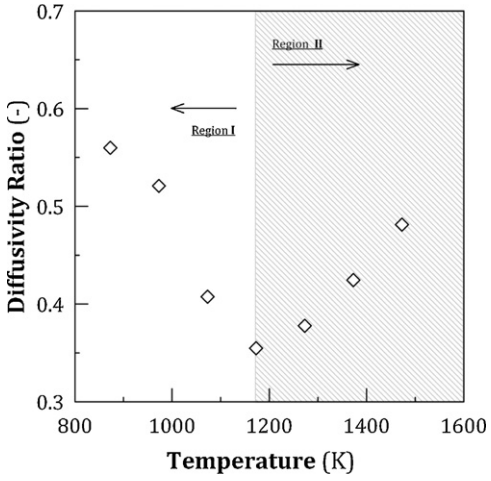

Fig. 9. Oxygen ion diffusivity ratios of the P-07-YSZ to M-07-YSZ models at different temperatures.

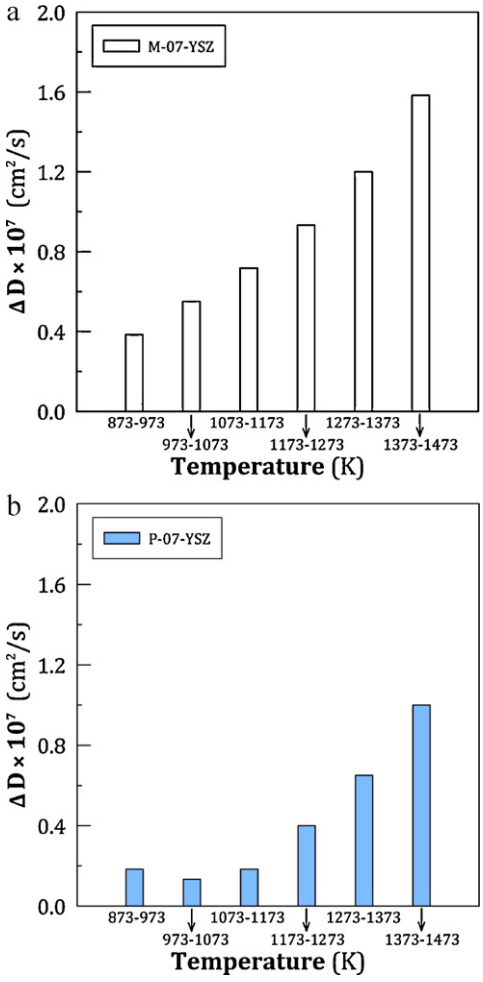

Fig. 10. Differences in the oxygen ion diffusivity of the (a) M-07-YSZ and (b) P-07-YSZ models at each temperature interval from 873 K to 1473 K.

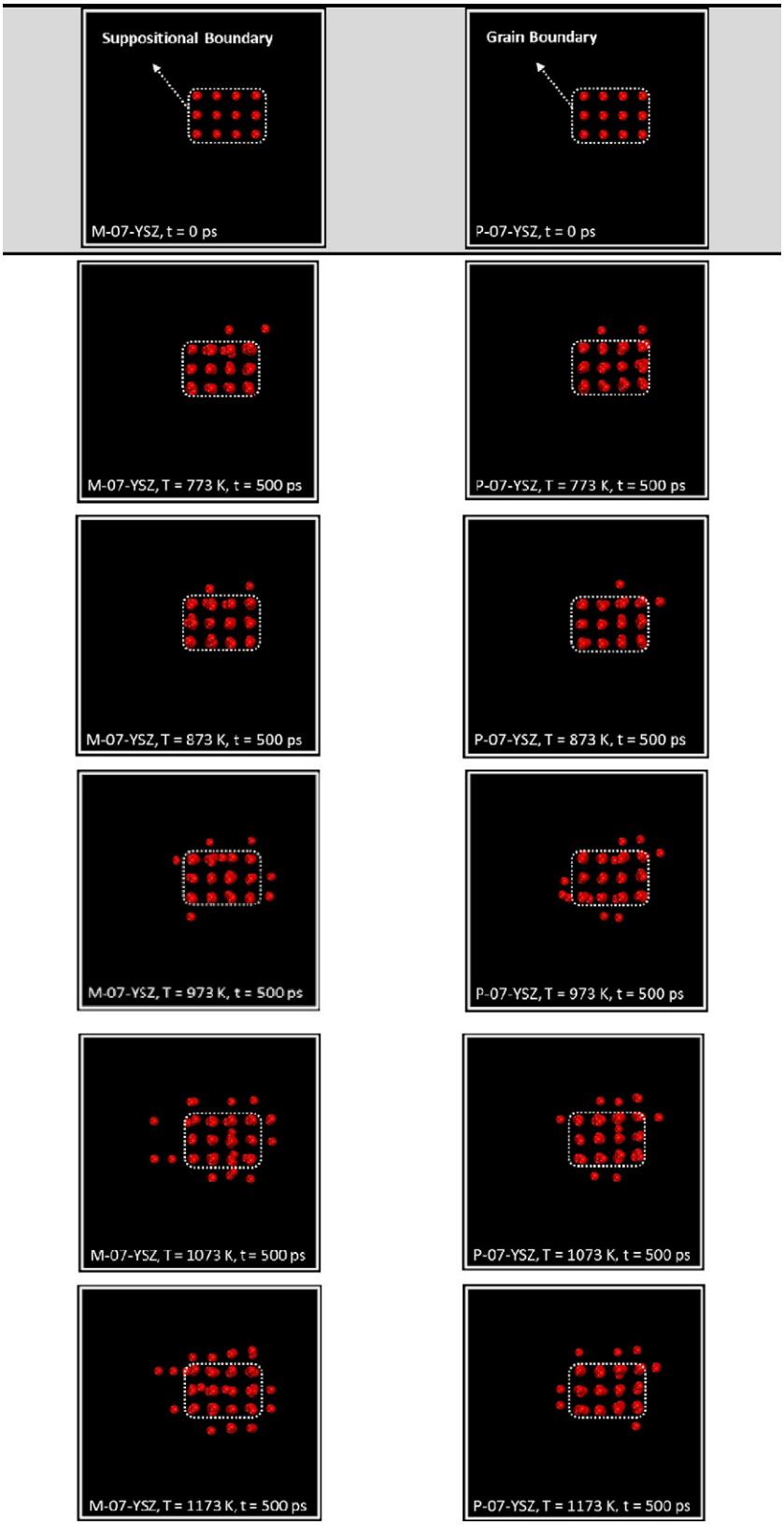

Fig. 11. Traveling trajectories of oxygen ions in M-07-YSZ and P-07-YSZ models from 773 K to 1473 K.

oxygen ion diffusivities of the two investigated models at different temperatures. Fig. 9 illustrates the diffusivity ratios of oxygen ions in the M-07-YSZ and P-07-YSZ models. The diffusivity ratio indicates the variation in ion diffusivity between the ideal and GB-inserted models. When this ratio approaches unity, it implies that the GBs have no effect on ionic transport (no difference between the M-07-YSZ and P-07-YSZ models); however, a decreased ratio suggests that the GBs in the P-07-YSZ model do affect ionic transport. In Fig. 9, the diffusivity ratio was first decreased (in Region I) and then increased (in Region II) by elevating the operational

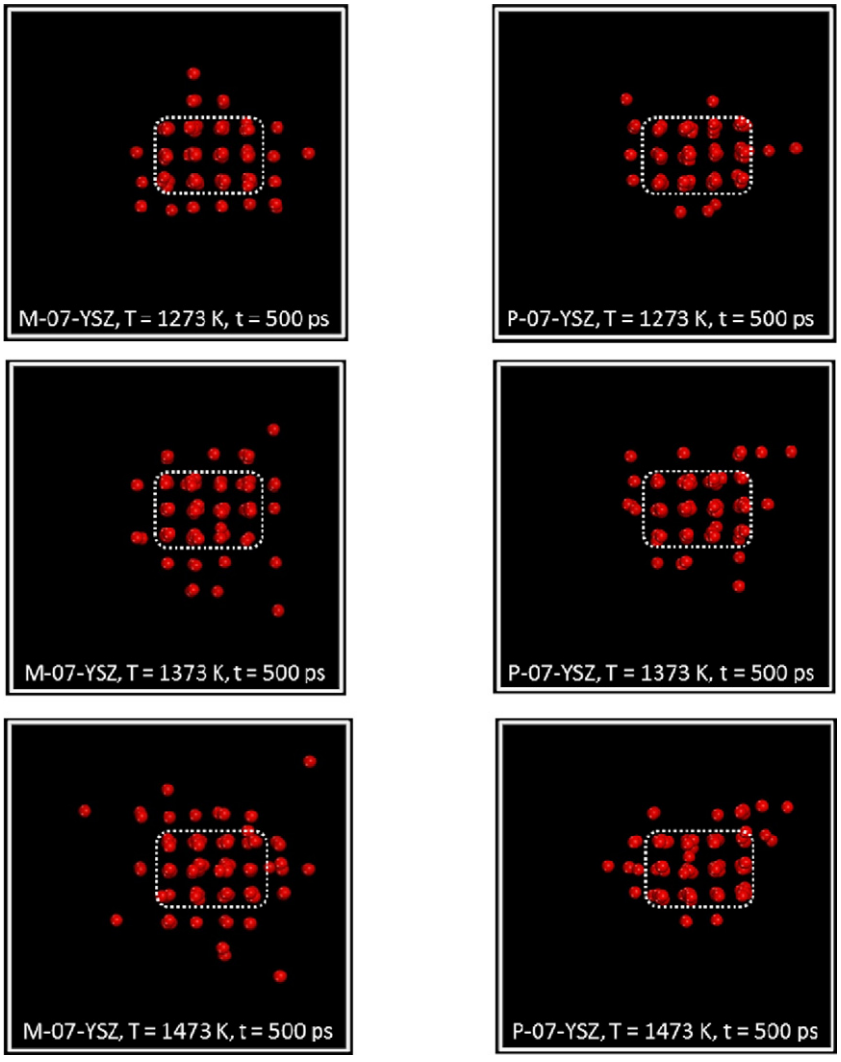

Fig. 11. (*continued*).

temperature. This change in diffusivity ratio might be explained by the following phenomenon. In real YSZ-based materials, the energy barrier to ion transport can be classified into two categories: dissociation energy and migration energy [36]. The dissociation energy indicates that the ions/vacancies that are bound to the surrounding ions trap the ions/vacancies. The ion can leave the trapped center when it acquires sufficient energy such that it can break away from its bound state. The migration energy indicates that the energy barrier that is formed by the resistance of ions that travel between the two sites might be formed by an intrinsic transport resistance, geometric structural factors (such as the presence of a GB), unfavorable phase structures, or some defects in the system. In Region I (lower temperature), the defect complexes consist of vacancies and doped cations with high binding energies that lower vacancy mobility. These defect complexes tend to accumulate near the GBs, which also increase the resistance. Meanwhile, the energy barrier of oxygen ions moving from one site to another would also be higher. Increasing the operational temperature increases the number of ions that would interact with GBs, which reflects the influence of GBs on diffusivity. Thus, the influence of GBs on ion transport in the P-07-YSZ model gradually increased with increasing temperature in Region I, which was reflected by the reduced diffusivity ratios. In Region II, the elevated temperature provides more kinetic energy to the vacancies, which may decrease the frequency of defect complex formation. Meanwhile, ions with higher velocities were able to overcome the GB-induced geometric resistance. Therefore, as the system was heated to specific temperatures, the associated mass transport resistances may have changed. The GB-induced oxygen ion migrational energy barrier could be gradually reduced as a result of (a) the 'decomposition' of defect complexes in the system (including those near the GBs) and (b) increased ion mobility at higher temperatures. In other words, the impact of GBs on ion transport gradually decreased in the P-07-YSZ model at elevated temperatures in Region II. As a result, the diffusivity ratio tended to increase with increasing temperature in Region II. This phenomenon of a reduced impact of GB on ion transport at high temperatures also agrees well with previous experimental results [4,10,16].

In addition, we also estimated the difference in ion diffusivities between the two specific temperatures, e.g., $\Delta D_{873-973} = D_{973} - D_{873}$, wherein D_{873} and D_{973} are the diffusivities of oxygen ions at 873 K and 973 K, respectively, as shown in Fig. 10. As shown in Fig. 10(b), the ΔD values tended to be maintained or slightly reduced at low temperatures and increased at high temperatures in the P-07-YSZ model. This tendency illustrates that the improvement in ion diffusivity via heating at low temperatures was limited because of the apparent effect of GBs. Meanwhile, the ΔD values in the P-07-YSZ model increased at higher temperatures because the mass transport barrier was reduced in the absence of GB resistance; however, the ΔD values

in the M-07-YSZ model continuously increased throughout the entire investigated temperature range, which indicates that the ideal YSZ model only revealed the mass transport resistance of the GI. Thus, the ΔD values were monotonically increased by the heating treatment and did not indicate the impact of the added GBs.

3.4. Oxygen ion traveling trajectory

We also observed the ion traveling trajectories of M-07-YSZ and P-07-YSZ models during the 500-ps MD duration at different temperatures, as Fig. 11 shows. In Fig. 11, we selected several oxygen ions in both YSZ models. The initial positions of these ions were set as the same coordinates for comparing their trajectories. The first row shows the ion positions of YSZ models at the initial point of the MD calculation, i.e., $t = 0$ ps. The following rows show the ion positions of YSZ models after 500-ps MD calculations. In other words, the images show the ion positions at $t = 500$ ps at various temperatures. In Fig. 11, it was found that the ions neither left the suppositional boundary (M-07-YSZ) nor the grain boundary (P-07-YSZ) while the temperature was below 973 K. This slight oxygen movement pointed out the minute ion mobility at low temperature. Furthermore, the ions started to show a clear migration behavior from 1073 K to 1274 K. The more drastic ion transport was elicited when the temperature was higher than 1373 K. Furthermore, it should also be noted that the difference in ion movements between M-07-YSZ and P-07-YSZ became much more obvious at higher temperatures, especially in the case of 1273 K, 1373 K, and 1473 K. The higher temperature made the GB effect easier to observe by tracing the ion positions. This temperature-dependent ionic transport agreed with the results of the diffusivity analysis that were described above (see Fig. 8).

4. Conclusions

In this work, a molecular YSZ model with added GBs was successfully constructed via an MD simulation technique. An increase in the Y_2O_3 concentration in YSZ released more vacancies but also lowered the accessible free space and vacancy mobility. These opposite tendencies caused by increasing the Y_2O_3 content led to an optimized YSZ concentration at 7 mol%. The presence of GBs in the YSZ structure resulted in degraded ion transport characteristics, which increased low-mobility ions and decreased continuous ion motions near the boundaries, resulting in lower ion diffusivities. The GB effect can be more easily observed at higher temperatures. From the ion diffusivity analyses, the GI and GBs dominate ionic transport at lower temperatures, whereas the influence of GBs was eliminated at higher temperatures because the migration energy barrier was overcome. The GB-inserted YSZ model can effectively simulate ionic transport through the GI and GBs, thus providing a more accurate methodology for predicting ionic transport behaviors in comparison with that achievable using a conventional ideal YSZ model.

Acknowledgements

Financial support from the Center-of-Excellence (COE) Program on Membrane Technology from the Ministry of Education (MOE), Taiwan, ROC and the National Science and Technology Program - Energy (Project number: NSC100-3113-E-033-001), the National Science Council (NSC), Taiwan, ROC are gratefully acknowledged.

References

[1] S.P.S. Badwal, F.T. Ciacchi, Adv. Mater. 13 (2001) 993–996.
[2] K.L. Tung, K.S. Chang, C.C. Hsiung, Y.C. Chiang, Y.L. Li, Sep. Purif. Technol. 73 (2010) 13–19.
[3] M. Hattori, Y. Takeda, Y. Sakaki, A. Nakanishi, S. Ohara, K. Mukai, J.H. Lee, T. Fukui, J. Power Sources 126 (2004) 23–27.
[4] S. Hui, J. Roller, S. Yick, X. Zhang, C. Deces-Petit, Y. Xie, R. Maric, D. Ghosh, J. Power Sources 172 (2007) 493–502.
[5] Z. Lv, R. Guo, P. Yao, F. Dai, Mater. Design 28 (2007) 1399–1403.
[6] Z.G. Lv, P. Yao, R.S. Guo, F.Y. Dai, Mater. Sci. Eng. A 458 (2007) 355–360.
[7] B. Bai, N.M. Sammes, A.L. Smirnova, J. Power Sources 176 (2008) 76–81.
[8] A. Martínez-Amesti, A. Larrañaga, L.M. Rodríuez-Martínez, N.M. Luisa, J.L. Pizarro, A. Laresgoiti, M.I. Arriortua, J. Power Sources 192 (2009) 151–157.
[9] F. Yang, X. Zhao, P. Xiao, J. Power Sources 196 (2011) 4943–4949.
[10] C. Hang, C.-J. Li, G. Zhang, X.-J. Ning, C.X. Li, H. Liao, C. Coddet, Mater. Sci. Eng. B 137 (2007) 24–30.
[11] Y.H. Koh, J.J. Sun, W.Y. Choi, H.E. Kim, J. Power Sources 161 (2006) 1023–1029.
[12] M.A. Laguna-Bercero, S.J. Skinner, J.A. Kilner, J. Power Sources 192 (2009) 126–131.
[13] B. Scherrer, A. Rossi, J. Martynczuk, M.D. Rossell, A. Bieberle-Hütter, J.L.M. Rupp, R. Erni, L.J. Gauckler, J. Power Sources 196 (2011) 7372–7382.
[14] B.K. Lai, K. Kerman, S. Ramanathan, J. Power Sources 196 (2009) 1826–1832.
[15] B. Kumar, C. Chen, C. Varanasi, J.P. Fellner, J. Power Sources 140 (2005) 12–20.
[16] X. Guo, R. Waser, Prog. Mater. Sci. 51 (2006) 151–210.
[17] Y.Z. Xing, C.J. Li, C.X. Li, G.J. Yang, J. Power Sources 176 (2008) 31–38.
[18] Y. Ji, J. Liu, Z. Lu, X. Zhao, T. He, W. Su, Solid State Ionics 126 (1999) 277–283.
[19] T.S. Zhang, S.H. Chan, W. Wang, K. Hbaieb, L.B. Kong, J. Ma, Solid State Ionics 180 (2009) 82–89.
[20] C.A.J. Fisher, H. Matsubara, J. Eur. Ceram. Soc. 19 (1999) 703–707.
[21] B. Zhu, S. Li, B.E. Mellander, Electrochem. Commun. 10 (2008) 302–305.
[22] K.S. Chang, T. Yoshioka, M. Kanezashi, T. Tsuru, K.L. Tung, Chem. Commun. 46 (2010) 9140–9142.
[23] K.S. Chang, Y.H. Huang, K.R. Lee, K.L. Tung, J. Membr. Sci. 354 (2010) 93–100.
[24] K.S. Chang, C.C. Hsiung, C.C. Lin, K.L. Tung, J. Phys. Chem. B 113 (2009) 10159–10169.
[25] T. Yoshioka, A. Yasumoto, K. Kishi, T. Tsuru, Desalination 233 (2008) 333–341.
[26] D. Hofmann, M. Entrialgo-Castano, A. Lerbret, M. Heuchel, Y. Yampolskii, Macromolecules 36 (2003) 8528–8538.
[27] S. Molin, M. Gazda, P. Jasinski, J. Power Sources 194 (2009) 20–24.
[28] X. Xie, R.V. Kumar, J. Sun, L.J. Henson, J. Power Sources 195 (2010) 5660–5665.
[29] F. Shimojo, H. Okazaki, J. Phys. Soc. Jpn. 61 (1992) 4106–4118.
[30] F. Shimojo, T. Okabe, F. Tachibana, M. Kobayashi, H. Okazaki, J. Phys. Soc. Jpn. 61 (1992) 2848–2857.
[31] R. Devanathan, W.J. Weber, S.C. Singhal, J.D. Gale, Solid State Ionics 177 (2006) 1251–1258.
[32] M. Kilo, C. Argirusis, G. Borchardt, R.A. Jackson, Phys. Chem. Chem. Phys. 5 (2003) 2219–2224.
[33] S. Chen, D. Wang, M. Yu, B. Hu, X. Wang, Y. Liu, Y. Yin, Mater. Chem. Phys. 103 (2007) 28–34.
[34] W. Araki, Y. Arai, Solid State Ionics 181 (2010) 1534–1541.
[35] H. Ogawa, N. Sawaguchi, F. Wakai, Mater. Sci. Forum 243–245 (1997) 351–356.
[36] K.S. Chang, K.L. Tung, ChemPhysChem 10 (2009) 1887–1894.
[37] C.A.J. Fisher, H. Matsubara, Solid State Ionics 113–115 (1998) 311–318.
[38] C.A.J. Fisher, H. Matsubara, Comput. Mater. Sci. 14 (1999) 177–184.
[39] G.V. Lewis, C.R.A. Catlow, J. Phys. C: Solid State Phys. 18 (1985) 1149–1161.
[40] A. Dwivedi, A.N. Cormack, Philos. Magn. A 61 (1990) 1–22.
[41] G.E. Murch, Solid State Ionics 7 (1982) 177–198.
[42] X. Li, B. Hafskjold, J. Phys. Condens. Matter 7 (1995) 1255–1271.
[43] Y. Arachi, H. Sakai, O. Yamamoto, Y. Takeda, N. Imanishai, Solid State Ionics 121 (1999) 133–139.